

SEGMENTATION OF BREAST CANCER MASSES IN ULTRASOUND USING RADIO-FREQUENCY SIGNAL DERIVED PARAMETERS AND STRAIN ESTIMATES

Etienne von Lavante, J. Alison Noble

University of Oxford
Wolfson Medical Vision Laboratory

ABSTRACT

In order to address the tendency of ultrasound B-Mode images to show a too small sizing of tumour masses in breast cancer diagnosis, a novel segmentation method has been introduced. In this paper it has been explored if this problem can be solved by incorporating strain parameters from ultrasound elastography into a segmentation framework. By incorporating a local power estimate from an autoregressive model on the RF-data with strain parameters into a fast algorithm using Graph-cuts, very difficult to interpret cancer data could be segmented successfully with more accurate sizing than with B-Mode data alone. However, more research is necessary to correlate histology findings with elasticity parameters to find the best model to interpret strain data for breast mass segmentation.

Index Terms— Biomedical acoustic imaging, Cancer, Image segmentation, Spectral analysis, Strain

1. INTRODUCTION

Ultrasonic imaging has become an indispensable tool used in diagnosis of cancer masses. However, despite its central role in breast cancer diagnosis, even for skilled radiologists it is still a challenging problem to correctly size and characterize cancer masses. The main challenges of sizing breast cancer masses in ultrasound is the lack of clear defined borders due to its invasive nature into healthy tissue, often a lack of distinctive texture compared to healthy tissue, irregular shape, anisotropic appearance and high cross-patient variability in texture and appearance. Naturally, the usual problems of ultrasound such as low contrast, speckle-, attenuation- and shadowing artefacts also have to be dealt with. In order to deal with these problems, we propose in this paper a novel method to segment breast masses using a combination of a RF-data derived measure and strain imaging parameters.

With other applications of medical ultrasound, segmentation algorithms have already shown great promise to help radiologists in the identification of image features. Some examples of effective segmentation frameworks are the work

by Xie et al[1] and Mulet-Prada[2] for kidney and cardiovascular segmentation, respectively. However, due the above mentioned challenges in the identification of breast cancer masses, such methods which rely on shape and texture priors or edge information can work poorly with breast ultrasound data. Hence, region based segmentation algorithms, usually based on Bayesian frameworks [3] or local image statistics [4], have been proposed for the problem of breast cancer segmentation.

However, segmentation based solely on static data is an extremely difficult problem. Correspondingly, radiologists rely on the utilization of dynamic information such as the stiffness and mobility of lesions for characterizing and sizing breast cancer. This is usually achieved by palpation, and the quantitative equivalent to this for the medical imaging community is ultrasound strain estimation (elastography). According to [5] the strain can be estimated with these methods accurately qualitatively and within a cumulative variance over time quantitatively.

So far the only attempts at segmentation based on parameters derived from the acoustic RF-signal are the works by Boukerroui[3] and Dydenko[6]. Of these works, only the work by Dydenko[6] is based solely on parameters derived from the RF-signal, using spectral autoregressive and velocity-based parameters for the segmentation of cardiographic images. The work by Boukerroui[3] is a hybrid B-mode RF-signal framework which uses the RF-signal to estimate parameters related to the local power of the signal (integrated backscatter and mean central frequency).

2. METHOD

2.1. Method - Overview of Graph-Cuts

We propose a region based segmentation framework using Graph-cuts that minimizes an energy function $E(x)$ of the following form:

$$E(x) = \theta_{\text{const}} + \sum_{p \in \mathcal{V}} \theta_p(x_p) + \sum_{(p,q) \in \mathcal{E}} \theta_{pq}(x_p, x_q) \quad (1)$$

Here, set \mathcal{V} corresponds to the set of pixels in the image; x_p denotes the label of pixel $p \in \mathcal{V}$ and the set \mathcal{E} corresponds to

Research supported by UK EPSRC Grant GR-S94575 01

the set of connections/edges each pixel p has with its neighbors q . The term θ_p encodes the cost functions associated with each label x and the pairwise term θ_{pq} is regularizing term penalizing differences in neighboring pixel intensities. For finding the global minimum of $E(x)$ in a binary segmentation one can use with Graph-cuts the very efficient and fast max flow-min cut algorithm[7]. This is a particularly attractive method for RF analysis due to the large volume of data.

Each edge of a pixel to its neighbors contains the similarity measure θ_{pq} , which gives a high cost when assigning two similar neighboring pixels different labels. In order to guarantee convergence, θ_{pq} has to be a submodular function satisfying:

$$\theta_{pq}(0,0) + \theta_{pq}(1,1) \leq \theta_{pq}(1,0) + \theta_{pq}(0,1) \quad (2)$$

Regarding this condition, the following cost function has been used in an eight pixel neighborhood:

$$\theta_{pq} = w_e \cdot e^{-\frac{(I_p - I_q)^2}{\rho}} \quad (3)$$

with I_q and I_p being the pixel intensities; ρ determining the cut-off value to penalize the difference between I_p and I_q and w_e being any positive value.

2.2. Method - RF Parameters

In prior work we used the residue r_p of an AR-model, as an estimate of power which is hardly affected by harmonic leakage and rarefaction artefacts[8]. As one can see in Fig. 1(b), the image from plotting this parameter has no visible speckle artefacts and its grey-level values can be directly used for segmentation.

For simplicity, a Gaussian mixture model is assumed for classifying the grey-level intensities of r_p into foreground x_{fgnd} and background x_{bgnd} . As presented in Fig. 2(a), a comparison of the histogram of an area within a cancer mass and an area of "normal" tissue shows sufficient distance between the peaks on the respective histograms to allow a separation of both labels with a Gaussian mixture model.

Being an estimate of the signal power, the residue-image r_p is naturally strongly effected by shadowing artefacts, causing the segmentation to bleed into the posterior shadow of cancer masses. To minimize this effect, a filter is applied to enhance any horizontal image features which might help to stop bleeding. Shown by Czerwiniski[9], the sticks filter is an optimal filter to identity linear features, and consequently r_p is convolved with such a filter f_{sticks} "tuned" to horizontal structures. Hence, one can model the cost function for both t-links as:

$$\begin{aligned} \theta_p(x_{\text{fgnd}}) &= w_f \cdot \phi_{\mu_f, \sigma_f^2}(r_p \star f_{\text{sticks}}) \\ \theta_p(x_{\text{bgnd}}) &= w_b \cdot \phi_{\mu_b, \sigma_b^2}(r_p \star f_{\text{sticks}}) \end{aligned} \quad (4)$$

Here, $\phi_{\mu_b, \sigma_b^2}(p)$ is the probability density function of a normal distribution with μ_f , μ_b , σ_f and σ_b as the mean and standard

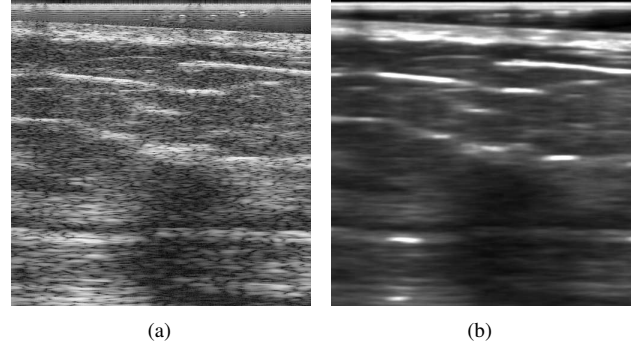


Fig. 1. The residue image (b) derived from the B-mode image (a). The image intensities of (b) are used to segment the mass in the center of the lower half of the image.

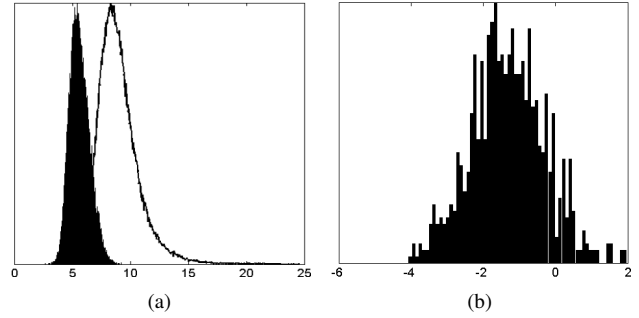


Fig. 2. Histograms of (a) the residue image, with the shaded plot being from a cancer mass; (b) strain in cancer mass

deviation of foreground and background image patches. With \star being the convolution operator, w_f , w_b being weighting factors, which are currently set to $w_f = w_b$ and can be any value greater than one.

2.3. Method - Strain Data

As it has been mentioned in the introduction, using eq.(4) will still not properly account for the problems of posterior shadowing and the invasive nature of cancer. Unfortunately, there is little experience in the interpretation of the strain data from mammary ultrasound. The strain appears to be in Fig. 2(b) roughly Gaussian distributed, when measured within a well defined cancer mass. However, there is currently very little data available on the confidence intervals on where exactly the border of the cancer mass is, hence what the variance of the strain within a tumour mass is.

In the employed elasticity reconstruction algorithm, the strain of the tumour mass is defined by design at around 0% relative strain. Correspondingly, the foreground strain cost

function $\psi_f(s_p)$ can be defined as a normal distribution with $\mu = 0$ and σ_s^2 estimated from the data. The background of the strain image consists mainly of two different structures: normal fatty breast tissue and the pectoral muscle. Normal tissue will show high relative strain as it is softer than tumour masses, and muscle tissue will show very low relative strain. Using this information it the background strain cost function $\psi_b(s_p)$ is defined as the inverse of the foreground cost function. This can be achieved for example by taking the *log* of $\psi_f(s_p)$, which will yield the final cost functions:

$$\begin{aligned}\theta_p(x_{\text{fgnd}}) &= w_f \cdot \phi_{\mu_f, \sigma_f^2}(r_p \star f_{\text{sticks}}) + w_{sf} \cdot \psi_f(s_p) \\ \theta_p(x_{\text{bgnd}}) &= w_b \cdot \phi_{\mu_b, \sigma_b^2}(r_p \star f_{\text{sticks}}) + w_{sb} \cdot \psi_b(s_p)\end{aligned}\quad (5)$$

with

$$\begin{aligned}\psi_f(s_p) &= \phi_{0, \sigma_s^2}(s_p) \\ \psi_b(s_p) &= n \log(\psi_f(s_p) + \delta)\end{aligned}\quad (6)$$

and s_p being the strain at pixel p , δ being a small value and n being a normalisation factor.

3. IMPLEMENTATION

As the authors were not aware of any phantoms which reproduce the invasive nature of cancer into normal tissue, it was chosen to test the algorithm solely on already recorded patient data. All data was recorded during a breast cancer study, on an Analogic AN-2300 with a BK-Medical 8805 probe using a centre frequency of 4.0 MHz, and recording the RF-data at a sampling frequency of 40 MHz. The motion data for the strain reconstruction was recorded from an assisted freehand set-up. All segmentation code was written in C++ using the ITK libraries for general image processing and code from V. Kolmogorov for the max-flow min-cut algorithm.

4. VALIDATION

Currently most cancer cases detected by the above mentioned study have been treated with an wide area local excision (cutting the tumour out). Consequently, there are from pathology histology slides of the removed cancer available, which shows the biological ground truth on tumour growth. As these slides are always cut along the superior-inferior axis from superficial to deep, one can measure the ground truth on the maximum tumour size along these two planes. To correlate the histology findings with the ultrasound data, a scanning procedure was employed where the ultrasound probe is aligned along the same plane as the histological slides are cut, and the radiologist scans once in this orientation the maximum tumour extent along the superior-inferior and once along the superficial-deep plane. In both scans the radiologist then sizes the tumour along the appropriate axis to obtain the B-mode sizing data. These same scans will be segmented with the above algorithm and then compared with the B-mode and histology sizing.

5. EXPERIMENTAL RESULTS AND DISCUSSION

Due to the large time delay between the screening, operation and then pathological analysis of the excised tumour, so far only four pathological reports have become available from patients scanned with the procedure from section 4. An overview of the current sizing results can be seen in figure 3(d), where for each patient the first column represents the superior-inferior sizing and the second one showing superficial-deep measurements.

As it has been experienced regularly in clinical practise, most B-mode measurements under represent the true size of the tumour mass. With the greatest discrepancy being with patient 2, showcased in figure 3(a) for the B-mode sizing and 3(b) for the corresponding segmentation result. Another interesting feature of this case is the presence of a very large ductal carcinoma in situ (DCIS), benign abnormal growth, outside of the main invasive tumour site. The sizing of the DCIS is according to histology 25mm, and can be seen as the large spiculations to the right of the main mass. As the DCIS has to be removed as well, the oversized segmentation is actually the clinically relevant sizing of the tumour. Despite this, the measurements on figure 3(d) for this case are without the DCIS.

Regarding the other measurements, the general trend is that B-mode sizing measurements are too small and the segmentation results are always larger than the B-Mode estimate and are mostly roughly 1mm larger than histology measurements. As having a too small sizing estimate is clinically dangerous, the segmentation results are in all cases the safer and preferred estimate for the planning of treatment and surgery. Regarding the segmentation sizing, it has to be noted that one could get more accurate results if one changed by hand for each case the mean and variance of $\psi_f(s_p)$ to account for noise in the strain data. The absolutely accurate results for patient 2 is due to the high quality of the strain estimate, which can be seen in figure 3(c). Hence, the need for more research into dealing with noise in strain data is required. Despite this, the sizing from the segmentation is already more accurate and clinically more relevant and safer than the sizing a trained radiologist could ever do with B-Mode data alone.

6. CONCLUSION

In this paper it has been explored how incorporating strain parameters into a Graph-cuts based segmentation algorithm will improve the sizing of tumour masses in ultrasound. Due to the high time delay between initial diagnosis and pathological analysis of the excised tumour, only a very a small number of cases are present where the sizing data can be compared with the ground truth from histology. Even with this small data set there is already a clear trend of the segmentation always delivering a clinically safer and in most cases a more accurate sizing estimate than a trained radiologist could do

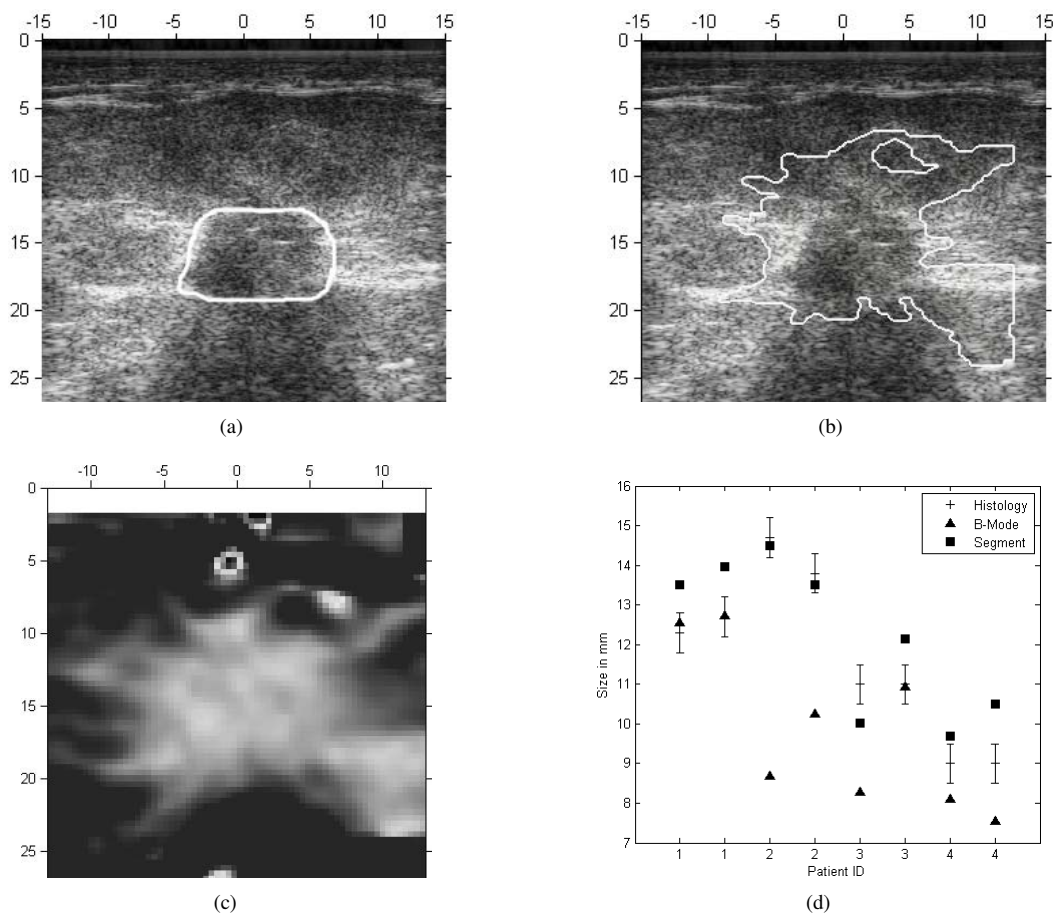


Fig. 3. Overall sizing results are shown in (d) with for each patient the first column showing inferior-superior and second one superficial-deep sizing, (a) B-mode sizing of patient 2, (b) corresponding segmentation result, (c) corresponding strain data

with B-Mode data alone. However, better understanding of how strain data correlates with histology is required to obtain more accurate results.

7. REFERENCES

- [1] J. Xie and et al., "Segmentation of kidney from ultrasound images based on texture and shape priors," *IEEE Trans Med Imag*, , no. 1, pp. 45–57, 2005.
- [2] M. Mulet-Parada and A. J. Noble, "2d+t acoustic boundary detection in echocardiography," *Medical Image Analy*, , no. 1, pp. 21–30, 2000.
- [3] D. Boukerroui and et al., "Segmentation of ultrasound images - multiresolution 2d and 3d algorithm...", *Pattern Recognition Letters*, , no. 4, pp. 779–790, 2003.
- [4] A. Madabhushi and et al., "Combining low-, high-level and empirical domain knowledge...", *IEEE Trans Med Imag*, , no. 2, pp. 645–632, 2003.
- [5] Z. Qian and et al, "Ultrasound myocardial elastography and registered 3d tagged mri...", *MICCAI*, 2007, vol. I, pp. 800–808.
- [6] I. Dydenko and et al., "Towards ultrasound cardiac image segmentation beased on the radiofrequency signal," *Medical Image Analy*, pp. 353–367, 2003.
- [7] V. Kolmogorov and R. Zabih, "What energy funtions can be minimized via graph cuts," *IEEE Trans Pattern Analy Mach Intel*, vol. 26, no. 2, pp. 147–159, 2004.
- [8] E von Lavante and J. A. Noble, "Improving the contrast of breast cancer masses...", *MICCAI*, 2007, vol. I, pp. 153–160.
- [9] R.N. Czerwiniski, D.L. Jones, and W.D. O'Brien, "Line and boundary detection in speckle images," *IEEE Trans Image Proc*, , no. 12, pp. 1700–1714, 1998.